كلية الهندسة بشبرا
FACULTY OF ENGINEERING AT SHOUBRA
ERJ
PRINT ISSN 3009-6049
ONLINE ISSN 3009-6022

ENGINEERING RESEARCH JOURNAL (ERJ)
Volume (54),Issue (1)
January 2025, pp:183-196
https://erjsh.journals.ekb.eg

Innovative Strengthening of Shear and Torsion Performance in Box-Section Concrete Beams with Near-Surface Mounted GFRP Rods

Moaz Abdel Nasser Mansour [1, 2,*] , Tarek S. Mustafa [1], Ahmed Mahmoud [1], Ahmed N Khater [1]

[1] *Civil Engineering Department, Faculty of Engineering at Shoubra, Benha University, Cairo, Egypt.*
[2] *Civil Engineering Department, High Institute for Engineering Technology, 21K Cairo, Belbies Rd., Al-Obour, Egypt.*
**Corresponding author*

E-mail address: eng_moaaz_civil@yahoo.com, tarek.mohamed@feng.bu.edu.eg, ahmed.ahmed@feng.bu.edu.eg, ahmed.khater@feng.bu.edu.eg

Abstract: The study of reinforced concrete (RC) hollow box-section beams reinforced with glass fiber-reinforced polymer (GFRP) bars and stirrups under combined shear and torsional stresses is still in its early stages, with the mechanisms of torsional failure not yet well-defined. This research examines the impact of adding external transverse strengthening to box-section beams, specifically utilizing GFRP rope as near-surface-mounted (NSM) external stirrups to enhance their structural performance. A total of nine RC box-section beams, each 2200 mm long, 400 mm wide, and 600 mm high, were constructed and tested under simply supported conditions. The study evaluated three variables: GFRP bar diameter, inclination angle, and spacing. Nonlinear finite element analysis was conducted using ANSYS to compare the behavior of these beams, internally reinforced with GFRP bars and stirrups, against beams externally strengthened with GFRP ropes as NSM stirrups. Three-dimensional finite element models were developed, incorporating a smeared cracking approach for the concrete and 3D elements. The analysis showed strong alignment between numerical results and experimental data through both linear and nonlinear phases up to failure, confirming the reliability of the model for future investigations. The findings demonstrated that integrating GFRP shear reinforcement, whether internally or externally, increased the load-carrying capacity by up to 45% relative to the control beam, depending on the variables studied.

Keywords: retrofitting; finite element analysis (FEA); box-section; near-surface-mounted (NSM); shear and torsion; glass-fiber-reinforced polymer (GFRP); GFRP ropes.

1. Introduction

Shear failure in concrete elements is particularly critical due to its sudden occurrence and lack of sufficient warning, often resulting from inadequate shear reinforcement, steel corrosion, exposure to harsh environmental conditions, freeze-thaw cycles, or corrosive chemicals [1]. Fiber-reinforced concrete (FRC) has emerged as a widely used construction material in various structural applications, such as industrial building slabs and concrete sewer pipes, owing to its enhanced shear resistance, including reductions in crack formation and shear crack widths, as highlighted in numerous studies [2-5].

Fiber-reinforced polymer (FRP), utilized in the form of reinforcement bars or sheets for strengthening beams, is increasingly recognized as an effective material for concrete rehabilitation. This is attributed to its unique advantages, including corrosion resistance, extended service life, resistance to humidity, high tensile strength, lightweight, durability, low maintenance requirements, ease of application, and nonmagnetic properties [6,7]. Replacing steel reinforcement with FRP bars, effectively addresses durability challenges in aggressive environments, such as roadbeds and bridge decks, where significant steel corrosion often occurs [8].

Extensive research [9] has been conducted on the use of various types and ratios of FRP bars in reinforced concrete beams without web reinforcement, analyzing their effects on shear capacity in comparison to conventionally reinforced steel beams. In studies investigating shear capacity, the near-surface mounted (NSM) and externally bonded reinforcement (EBR) techniques have been employed without incorporating discrete glass fibers in the concrete [10,11].

The NSM FRP method offers distinct advantages, such as eliminating the need for surface preparation [12,13], faster installation, protection against external factors (e.g., mechanical damage, vandalism, and fire), increased load-carrying capacity of reinforced concrete (RC) elements, and the ability to generate higher strain in FRP [14]. Additionally, it enhances confinement provided by the surrounding concrete and epoxy, thereby reducing the risk of debonding [15]. These attributes establish NSM as a superior alternative to traditional methods like EBR for strengthening RC structures.

Finite element (FE) modeling has been extensively employed in theoretical investigations of beams using various software tools, including ANSYS [16–21]. In this study, ANSYS Mechanical APDL software was utilized to develop an analytical model for simply supported GFRC beams without stirrups, subjected to four-point bending. The outcomes, including failure load, deflection, and load-mid-span displacement relationships, were presented, along with an analysis of crack propagation in the GFRC beams.

The behavior of reinforced concrete beams strengthened with FRP materials and other retrofitting techniques was analyzed [22] conducted a parametric analysis using finite element modeling with ANSYS to investigate the flexural and torsional performance of beams retrofitted with FRP bars. The results demonstrated significant improvements in flexural capacity and torsional resistance, highlighting the effectiveness of FRP for strengthening aging concrete structures.

Similarly, studied beams retrofitted with ferrocement and FRP materials under torsional loading through both experimental and numerical approaches. The findings revealed that FRP reinforcement notably enhanced torsional strength, with the FEM results closely aligning with experimental data, validating the accuracy of the computational methods [23].In another study, investigated the Near-Surface Mounted (NSM) technique for strengthening beams measuring 150x300x2000 mm using CFRP and GFRP bars. The strengthened beams exhibited increased stiffness, reduced deformation, and up to 60% improvement in flexural strength compared to control specimens, confirming the efficacy of NSM in enhancing structural performance [24].Collectively, these studies demonstrate the effectiveness of FRP materials and advanced retrofitting techniques in improving the structural integrity, flexural strength, and torsional resistance of reinforced concrete elements, making them reliable solutions for extending the service life of concrete structures.

2. Experimental program

2.1 Description of tested specimens

The experimental program involved casting and testing nine reinforced box-section beam specimens. One specimen served as the control beam, while the remaining eight beams were strengthened using near-surface-mounted (NSM) techniques with closed external stirrups. The study considered the following three primary variables:

a) GFRP bar diameter: Φ8, Φ10, and Φ12.
b) GFRP bar inclination: 60° and 90°.
c) GFRP bar spacing: 75 mm, 100 mm, 125 mm, and 150 mm.

Throughout the experimental investigation, the specimens' dimensions, clear span, concrete grade, loading locations, and longitudinal and diagonal reinforcement were kept constant [31].

The experimental work also included control tests on cubes and cylinders to assess parameters such as cracking load, ultimate load, failure modes, overall behavior, and stress-strain relationships. The beams were constructed and tested in the concrete laboratory at the Faculty of Engineering, American University in Cairo. To ensure uniform testing conditions, steel loading and bearing plates (400 × 100 × 50 mm) were placed at the loading and support points, while stiffeners made from solid reinforced concrete sections were used to prevent local failure at these points (see Figure 1).

The beam specimens were designed and analyzed in accordance with the Egyptian Code of Practice (ECP 208-2019) [34]. Since forming GFRP bars into stirrup shapes posed practical challenges, polypropylene elbows filled with epoxy resin were used as stirrups and tested for their effectiveness, as illustrated in Figure 2.

The experimental program was divided into three groups as follows:

Group 1: This group consisted of three specimens with varying shear spans of 600 mm, 450 mm, and 400 mm, corresponding to shear span-to-total depth ratios (a/t) of 1.0, 0.75, and 0.67, respectively, and an eccentricity-to-specimen width ratio (e/b') of 0.75. The control specimen, RB1, along with RB2 and RB3, were tested and subsequently strengthened using inclined stirrups at 45° with GFRP bar diameters of Φ8, Φ10, and Φ12, spaced at 100 mm (refer to Table 1).

Group 2: This group included three specimens with an eccentricity-to-specimen width ratio (e/b') of 0.75 and a shear span-to-total depth ratio (a/t) of 1.0. The strengthened specimens—RB7, RB4, and RB5—were reinforced using Φ10 GFRP stirrups spaced at 100 mm with inclinations of 45°, 60°, and 90°, respectively, over a shear span of 600 mm.

Group 3: This group comprised four specimens RB6, RB7, RB8, and RB9 designed with a shear span of 600 mm, equivalent to a shear span-to-total depth ratio (a/t) of 1.0, and an eccentricity-to-specimen half-width ratio (e/b') of 0.75. These specimens were strengthened using 45° inclined external stirrups, with spacing of 75 mm, 100 mm, 125 mm, and 150 mm [28].

The results of these tests were documented, analyzed, and compared, providing insights into the effects of the strengthening configurations on parameters such as carrying capacity, cracking behavior, failure modes, and ductility. This detailed investigation offers valuable information for designing effective shear and torsion strengthening techniques using NSM GFRP stirrups.

2.2 Test setup, instrumentation, and test procedure

The experimental procedures were carried out in the laboratory of the Faculty of Engineering at the American University in Cairo. Measurements of deflection and vertical load were obtained using external devices, including linear variable differential transformers (LVDTs) and load cells, as shown in Figure 1.

Deflection was recorded at the mid-span of the beams using LVDTs with effective lengths of 50 mm and 100 mm. A hydraulic actuator applied a symmetrical two-point vertical load at a specified distance (a) (the shear span). Prior to testing, the load cell and LVDTs were calibrated by laboratory experts, ensuring accuracy. Initial values were reset to zero using laboratory software to eliminate any baseline discrepancies.

A data acquisition system was employed to record measurements at each incremental load step. Crack propagation was visually monitored during the loading process, and all beams were inspected under displacement-controlled testing conditions. This methodology ensured precise and consistent data collection while allowing detailed observation of beam behavior under load.

Table 1: Details of the tested specimens.

Before Strengthening												After strengthening			
Group No.	Specimen No.	a (mm)	(a/t) ratio (-)	e (mm)	(e/b`) ratio (-)	μ/μ max. (-)	A_f (mm²)	A_f' (No. Φ Dia.)	Internal Vl. Web RFT (mm)	Internal Hz. Web RFT (mm)	Effect	Diameter of external GFRP stirrups (mm)	Stirrup inclination externally (degree)	Stirrup spacing on the outside (mm)	external stirrups' effects
1	RB1	600	1	150	0.75	0.4	905.12	4Φ8	8	8	Shear-span to total depth	10	45	100	Diameter
	RB2	450	0.75									8			
	RB3	400	0.67									12			
2	RB4	600	1	100	0.5	0.4	905.12	4Φ8	8	8	Eccentricity	10	60	100	Inclination
	RB5			170	0.85								90		
3	RB6	600	1	150	0.75	0.4	905.12	4Φ8	10	8	Vertical web reinforcement	10	45	150	Spacing
	RB7								12	8				100	
	RB8								8	10	Horizontal web reinforcement			75	
	RB9								8	12				125	

Where:

b` 200 mm is half of the beam web width.

Vl. is the vertical web-reinforcement.

Hz. is the horizontal web-reinforcement.

RFT is the reinforcement.

A_f the primary tension FRP bar area.

A_f' The secondary compression FRP bar area.

μ the major reinforcement ratio of FRP bars is denoted by (A_f/b*d).

μ_{max} is the maximum reinforcement ratio according to ECP 208–2019[31].

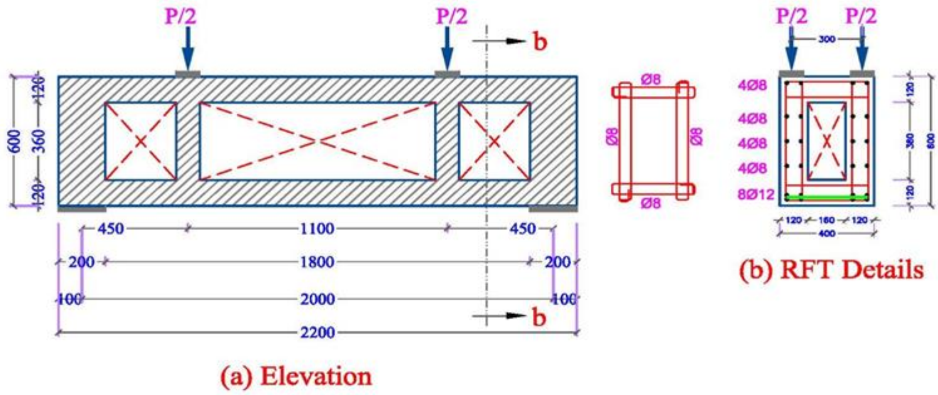

Figure 1 Typical specimen concrete dimension and reinforcement details

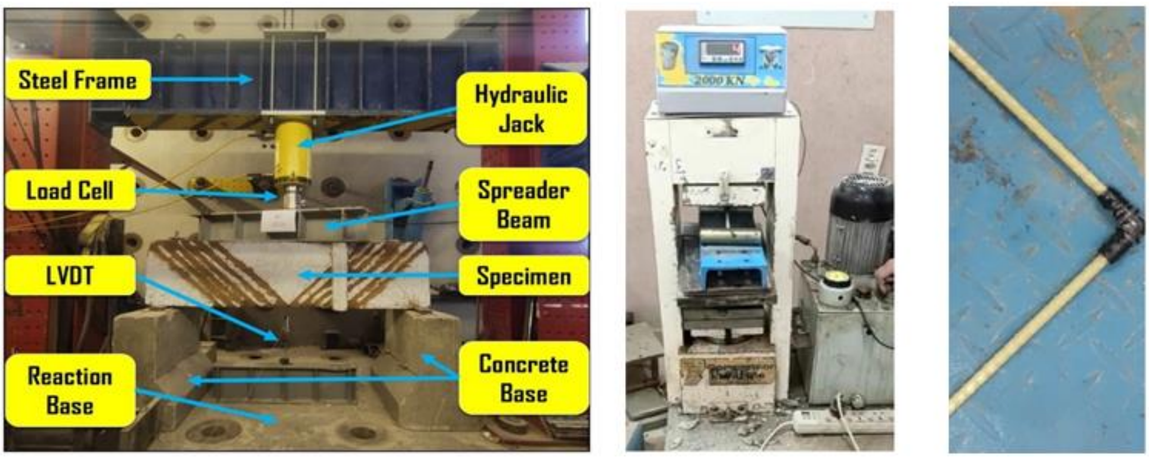

(a) Test setup **(b)** Stirrup elbow corner test **(c)** Stirrup corner connection (elbow)

Figure 2: Test setup and instrumentations.

2.3 Analysis of the Experimental Results

This study presents all the experimental results shown in table 2, such as (1) crack load P_{cri}; (2) failure load P_f; (3) the midpoint deflection at first crack and failure load Δ_{cri} and Δ_f, respectively; (4) crack patterns; and (5) failure modes. Tables. 2 show the experimental results for all the tested specimens after strengthen and tested.

Table 2: Experimental results for all the tested specimens after strengthening and testing.

Specimen No.	$P_{cr\,i}$ (kN)	P_f (kN)	$\Delta_{cr\,i}$ (mm)	Δ_f (mm)	S.S (kN/mm)	D.D (-)	T (kN.mm)	Failure mode
RB.1	568.1	731.4	11.53	16.64	54.60	2.13	3155.41	Diagonal shear failure mode
RB.2	554.9	658.9	10.05	12.21	29.02	1.65	5031.36	
RB.3	490.5	764.8	9.96	18.00	119.90	1.14	3846.74	
RB.4	543.8	655.2	12.60	16.55	19.71	1.71	5456.65	
RB.5	492.5	531.9	9.64	11.61	64.67	1.14	3818.48	
RB.6	591.2	649.9	12.53	15.80	51.17	1.62	4225.15	
RB.7	612.3	786.5	15.79	22.17	32.23	1.58	2731.72	
RB.8	631.2	822.4	13.88	23.83	36.39	1.15	2359.86	
RB.9	653.7	758.4	16.13	20.93	61.89	1.22	2130.18	

3. Spatial and Constitutive Models for Finite Element Analysis

3.1 Modeling of Concrete Material

Guided by the ANSYS R15.0 software manual [33], the concrete elements were modeled using the three-dimensional isoparametric element known as SOLID65. This element is capable of simulating both tension and compression cracking, as well as crushing behaviors in concrete. It is defined by eight nodes, each having three translational degrees of freedom along the x, y, and z axes, without any rotational degrees of freedom. A 2×2×2 Gaussian integration scheme was employed to determine the element stiffness matrix accurately.

The SOLID65 element can represent a single solid material—such as concrete—and accommodate up to three embedded reinforcing materials with different properties. Figure 2 illustrates the geometrical characteristics of the SOLID65 element. The analysis accounted for both linear and nonlinear behaviors of concrete. In the linear phase, concrete was assumed to behave isotropically until cracking occurred. For the nonlinear phase, a plasticity model was considered appropriate to represent the concrete's behavior.

Each integration point within the element can experience up to three orthogonal cracks. The ANSYS 15 software allows for the definition of steel reinforcement using the smeared reinforcement approach, where the reinforcement is specified by a volumetric ratio and the orientation angles of the rebars. For this purpose, the reinforcing bars were modeled using the LINK180 element.

The concrete model is specifically designed to predict the failure of brittle materials, encompassing both cracking and crushing modes. Figure 3,4 displays a three-dimensional failure surface within the principal stress space, illustrating the criteria for material failure used in the analysis.

The similarity angle η offers insights into the magnitudes of the principal stresses. Figure 5 presents the failure surface in the principal stress space, specifically for biaxial or nearly biaxial stress conditions. When the most significant non-zero principal stresses align with σ_{xp} and σ_{yp}, the represented surfaces correspond to σ_{zp} values slightly above zero, σ_{zp} equaling zero, and σ_{zp} slightly below zero. These three surfaces, when viewed as projections on the σ_{xp} - σ_{yp} plane, indicate a continuous three-dimensional failure surface. The material's failure mode is influenced by the sign of σ_{zp}. For example, if both σ_{xp} and σ_{yp} are negative and σ_{zp} is slightly positive, the prediction leans toward cracking perpendicular to σ_{zp}. On the other hand, if σ_{zp} is zero or slightly negative, the material's anticipated behavior is crushing.

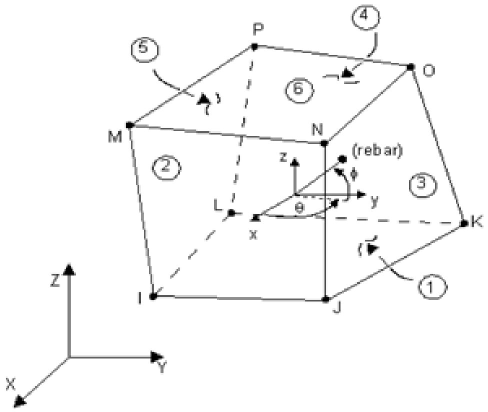

Figure 3 Geometry of 3-D Solid-65 element (concrete element).

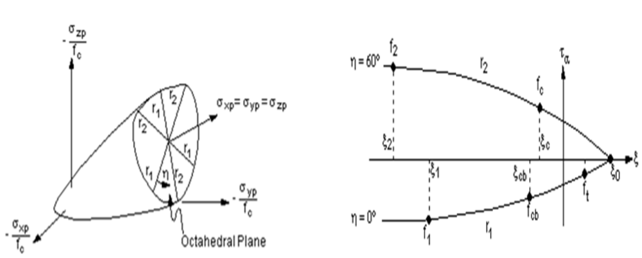

Figure 4 Three-dimensional failure surface of concrete material and its profile

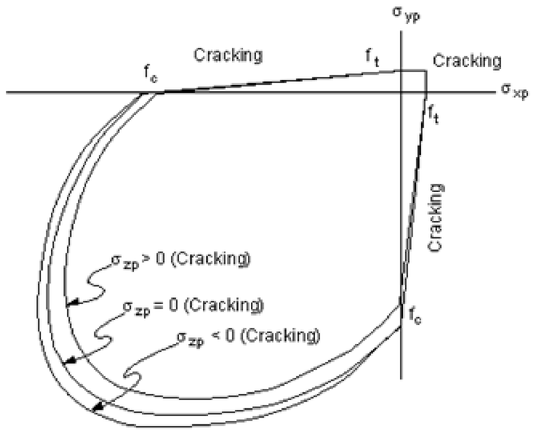

Figure 5 Concrete failure surface in principal stress space with biaxial stress

In establishing the failure surface and characterizing the tri-axial stress state, essential input strength parameters such as f_t, f_c, f_{cb}, f_1, and f_2 must be specified. The ultimate uniaxial compressive strength, fc, was derived from the experimental outcomes of cubic concrete samples associated with each beam specimen. Additionally, f_t was determined in accordance with ACI standards, specifically set at 0.1 times f_c. The remaining parameters were assigned default values as recommended.

$$f_{cb} = 1.2\, f_c\,,\ f_1 = 1.45\, f_c\,,\ \text{and}\ \ f_2 = 1.725\, f_c \tag{1}$$

Additional concrete material information is required, including idealized stress-strain relationship (Figure 5) according to ECP-203-2019 [35], elastic modulus (E_c) which was defined by Martinez S. et al. (1984) [32] in Eq. 2, shear transfer coefficient for closed and open cracks, tensile stress, and compressive stress.

$$E_c = 3320\sqrt{f_c'} + 6900 \text{ (MPa)} \tag{2}$$

The shear transfer coefficient is a critical parameter in modeling cracked concrete behavior, typically ranging from 0.0 to 1.0. A coefficient of 0.0 represents a completely smooth crack with no shear transfer, whereas a value of 1.0 signifies a highly rough crack capable of full shear transfer. This coefficient is applied to both open and closed cracks to define their respective shear transfer capacities.

In this study, the shear transfer coefficient for open cracks was set at 0.2, reflecting minimal shear transfer. For closed cracks, the coefficient was assigned a value of 0.8, indicating a relatively higher shear transfer capacity.

Additionally, a value of 0.6 was adopted to account for stress relaxation after cracking, following the recommendations outlined in the software package's technical guidelines. This approach ensured a realistic representation of the post-cracking behavior in the finite element analysis.

The selected coefficients, derived from a correlative study, were found to contribute to improved behavior in the tested beams, as evidenced by the analysis results. This demonstrates the importance of accurately defining shear transfer properties to simulate the structural performance of reinforced concrete elements effectively.

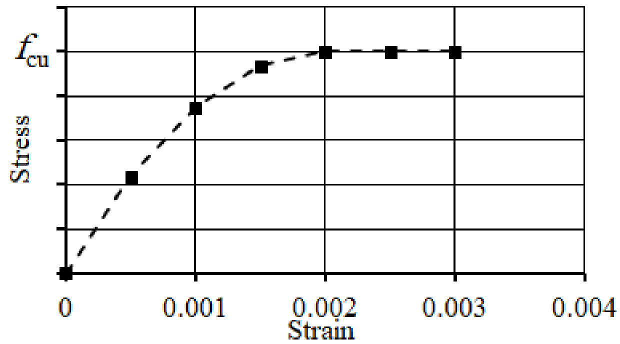

Figure 6 Idealized stress-strain curve for concrete in compression

Figure 6 depicts the simplified stress-strain relationship for concrete under compression and tension. The modulus of elasticity Ec, determined following the equation proposed by Martinez et al. [32].

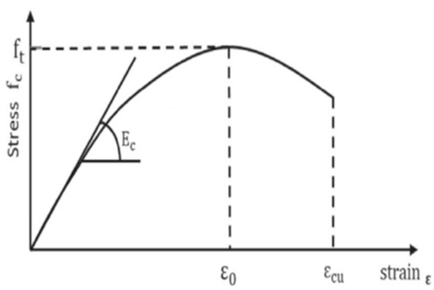

(a) Idealized stress-strain curve for concrete in compression.

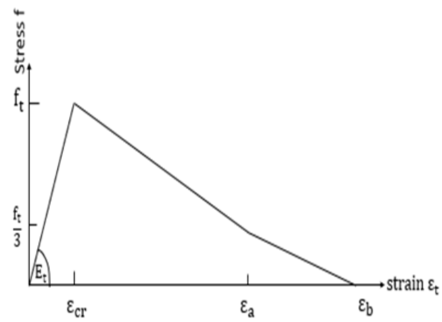

(b) Idealized stress-strain curve for concrete in tension.

Figure 7 Idealized stress-strain curve for concrete in compression and tension

3.2 Material Modeling of GFRP Reinforcement

Figure 7 Illustrates a bilinear stress-strain curve representing the idealized behavior of GFRP reinforcement obtained experimentally using ASTM D7205[36] and ASTM D790-02[37].

3.3 Analytical procedure

Nonlinear analysis was taken into account by using an incremental load process in the numerical solution scheme. Combining the economical nature of the modified Newton-Raphson approach, where the stiffness is reformulated at each load step, with the high convergence rate of the standard Newton-Raphson method, yielded an iterative solution that was done for each load increment. The convergence criterion utilized iterative nodal displacement, with only transitional degrees of freedom evaluated. The criterion is:

$$\Delta D / D \leq \lambda \quad (3)$$

Where (ΔD) is the iterative displacement norm and (D) is the total displacement norm. The acceptable range for the convergence tolerance (λ) was identified to be between 0.02 and 0.05, yielding reliable outcomes. If the convergence criteria were not met and numerical instability was exhibited, the load level was deemed the analytical ultimate load for the specimen.

Nonlinear analysis was conducted using an incremental load process within the numerical solution scheme. This approach combined the economic efficiency of the modified Newton-Raphson method, which updates the stiffness matrix at each load step, with the high convergence rate of the standard Newton-Raphson method. This hybrid method provided an efficient iterative solution for each load increment, ensuring stability and accuracy.

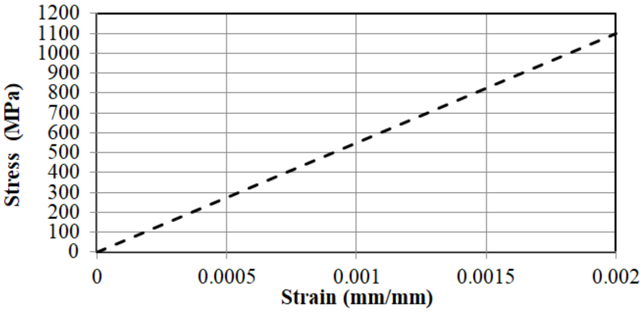

Figure 8 Idealized stress-strain curve for GFRP bars

3.4 Solution techniques

In this investigation, the shear transfer coefficient for open cracks (β_t) was set to 0.2, while for closed cracks (β_c), the value was within the generally accepted range of 0.8 to 0.9. This selection was informed by established guidelines and practical considerations for modeling cracked concrete behavior.

The numerical solution method employed an incremental load approach for the nonlinear analysis. Each load increment was processed iteratively, leveraging a hybrid approach that combined the computational efficiency of the modified Newton-Raphson method with the high convergence rate of the standard Newton-Raphson method, as outlined by Mahmoud [30].

Convergence was assessed using iterative nodal displacement, focusing exclusively on translational degrees of freedom. The convergence criterion was expressed as:

$\psi/R \leq \phi$ where: (ψ): Iterative displacement norm, (R): Total displacement norm .and (ϕ): Convergence tolerance.

The tolerance (ϕ) was maintained within the range of 0.02 to 0.05, ensuring reliable and accurate numerical outcomes. The numerical ultimate load was identified as the point of numerical instability, signifying the failure of the convergence condition and indicating the structural failure of the modeled specimen. This methodology ensured a robust and effective analysis of the nonlinear response of the tested beams.

4. Validation Studies

4.1 Studied model analysis

A comprehensive parametric investigation was conducted using the versatile computer software ANSYS V.15 [33]. The parameters under scrutiny encompassed various aspects, including concrete compressive strength f_c`, GFRP reinforcement ultimate strength f_u, and the primary GFRP reinforcement ratio μ, which was chosen for the parametric study, ensuring practical dimensions and properties, as depicted in Figures 9 and 10. The results were compared to the model in the experiment.

A comparative examination is conducted to validate the numerical model against experimental results, focusing on the load-deflection response, crack patterns, and failure modes. The experimental and numerical results are juxtaposed and compared, as depicted in Figures 8,9. Table 3 provides a comparison between the failure loads and deflections at the failure load of the tested beams between measured and predicted load-deflection curves. Further supporting the capability of the nonlinear finite element method using "ANSYS V.15 [33]" to accurately signify the behavior of these beams.

4.2 Geometry, modeling, loads, and boundary conditions

For the numerical modeling, the SOLID65 element was employed to model the concrete. This eight-node solid element includes three translational degrees of freedom (X), (Y), and (Z) directions) and additional rotational degrees of freedom at each node. The unique features of SOLID65, such as plasticity, cracking, creep, large strain, large deflection, and plastic deformation capability, were utilized to accurately simulate the behavior of concrete. The mesh size adopted for beam modeling was (50 × 50 × 50 mm), ensuring a balance between computational efficiency and result accuracy.

LINK180 elements were used to model the FRP bars and FRP stirrups. These elements are two-node elements with three translational degrees of freedom at each node (X), (Y), and (Z). A perfect bond was assumed between the FRP bars and the concrete, simplifying the interaction modeling and ensuring compatibility of displacements.

For the steel loading and bearing plates, SOLID185 elements were employed. These elements are suitable for modeling 3D solid structures and were used to simulate the behavior of the loading and support plates effectively. The arrangement and interactions of these elements are depicted in Figure 10, providing a comprehensive view of the modeling framework.

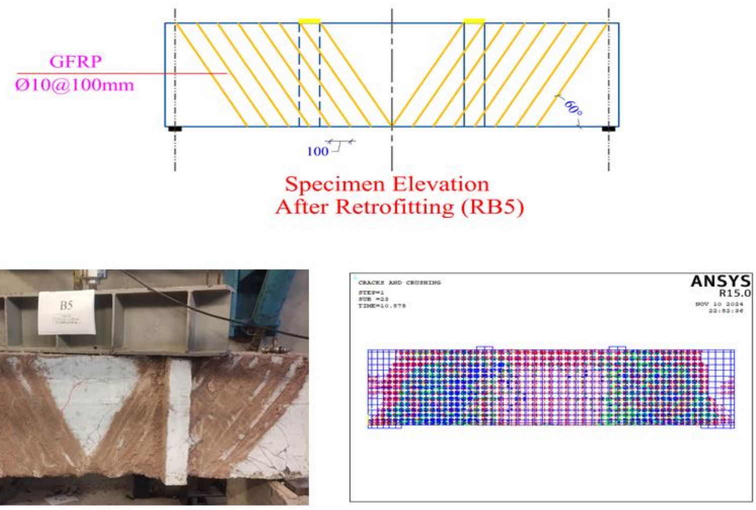

Figure 9 Parametric study for specimen RB5 after strengthen, experimental and numerical crack pattern

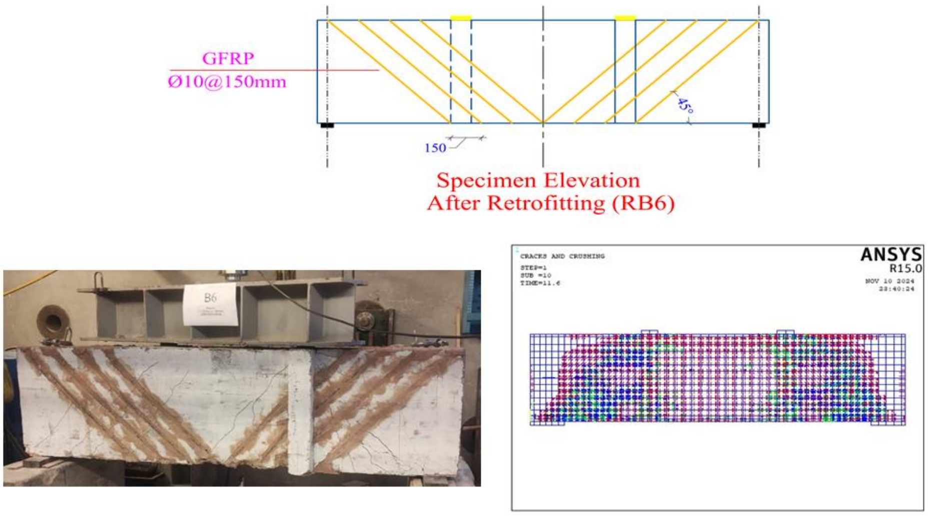

Figure 10 Parametric study for specimen RB6 after strengthen, experimental and numerical crack pattern.

Table 3: Comparison between experimental and numerical results for specimens RB5 and RB6 after strengthen.

Group no.	Beam no.	Failure load P_f (kN)			Deflection at failure load Δ_f (mm)		
		Numerical P_u	Experimental P_f	P_u/P_f	Numerical Δ_u	Experimental Δ_f	Δ_u/Δ_f
2	RB.5	525.23	531.87	0.99	11.15	11.61	0.96
3	RB.6	635.28	649.94	0.97	13.96	15.80	0.88

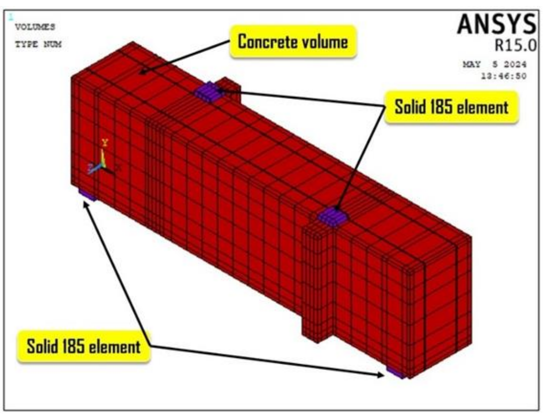

(a) Ansys modeling of the tested specimen

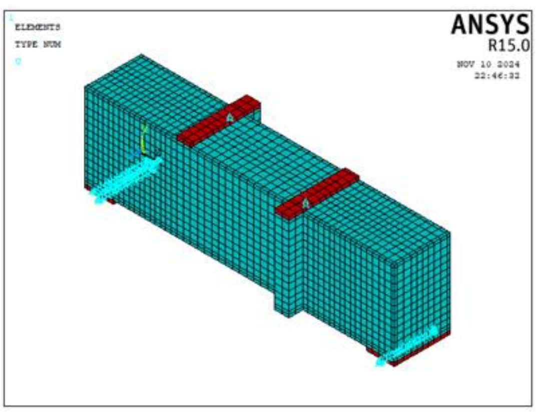

(b) Concrete, Loading And Bearing Plate Idealizations (3-D).

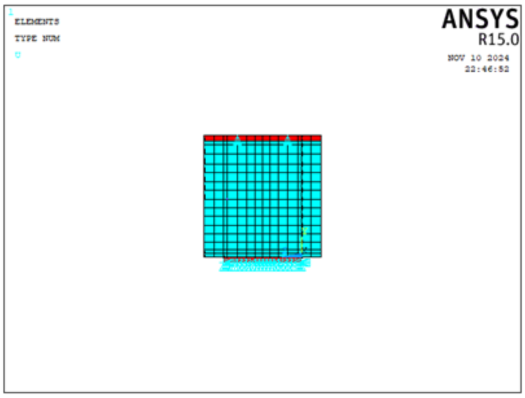

(c) Concrete, Loading And Bearing Plate Idealizations (side view 2-D).

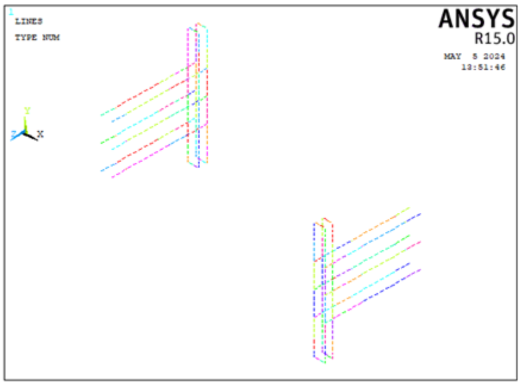

(d) Vertical And Horizontal GFRP Stirrups Branches.

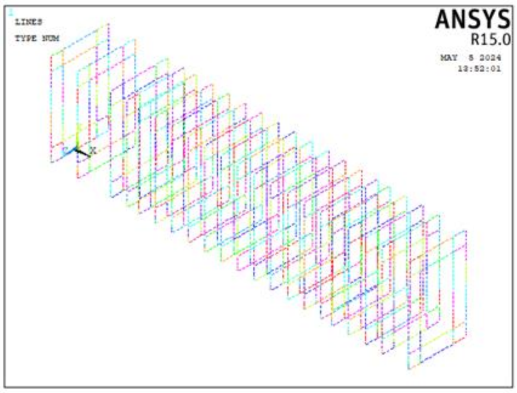

(e) Vertical And Horizontal GFRP Stirrups Idealizations

Figure 11 Idealization of the tested beams by ANSYS [30].

4.3 Ultimate Load Capacity Results

The ultimate capacity of the strengthened specimens was evaluated in figure 11, and the numerical results closely matched the experimental findings, reinforcing the reliability of the model in predicting failure load and deflection behavior. The coefficients of variation (C.O.V.) and mean ratios of numerical to experimental values indicate a high degree of accuracy across the parameters measured.

4.3.1 Detailed Specimen Analysis

- **Specimen RB5 (Group 2):** For RB5, the numerical ultimate load (P_u) was 525.23 kN compared to the experimental failure load (P_f) of 531.87 kN, yielding a ratio (P_u / P_f) of 0.99. This ratio demonstrates excellent alignment between the two, with a negligible variation. Similarly, the deflection at failure load was 11.15 mm (numerical) versus 11.61 mm (experimental), resulting in a deflection ratio (Δ_u/Δ_f) of 0.96. This minimal discrepancy in deflection measurements underscores the model's precision in capturing deflection responses under load.
- **Specimen RB6 (Group 3):** For RB6, the numerical failure load was 635.28 kN compared to an experimental value of 649.94 kN, producing a (P_u / P_f) ratio of 0.97, which is within an acceptable margin. The deflection ratio (Δ_u/Δ_f) of 0.88, based on 13.96 mm (numerical) and 15.80 mm (experimental), shows a slightly larger variation but remains within a consistent range, indicating a slight underestimation of deflection by the numerical model.

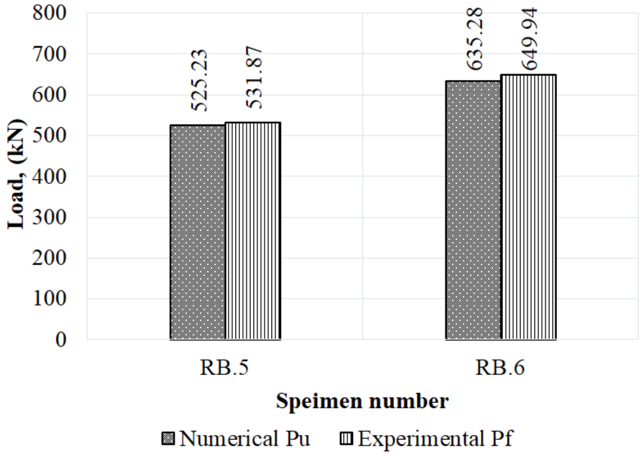

Figure 12 Experimental failure loads and numerical ultimate loads for two specimens

4.3.2 Load-deflection behavior

As shown in Figures 12 and 13, the nonlinear finite element analysis (NLFEA) effectively estimated the central deflection during the loading phases for most test specimens. However, the study encountered limitations in predicting the post-peak behavior for certain beams, particularly those that experienced sudden shear failure.

For the majority of cases, the NLFEA produced steeper load-deflection slopes compared to experimental results, indicating an overestimation of stiffness. This discrepancy is primarily attributed to the idealizations inherent in the finite element modeling, and to a lesser extent, potential overestimation of the concrete modulus of elasticity (E_c) used in the analysis.

Despite these limitations, the NLFEA closely replicated the observed experimental trends for ultimate load and peak central deflection. The use of ANSYS 15 [31] software demonstrated reliable performance in predicting load-bearing capacities, cracking behavior, and overall load-deflection responses across the investigated test parameters. This highlights the utility of NLFEA as an effective tool for analyzing the structural performance of reinforced concrete beams under varying conditions.

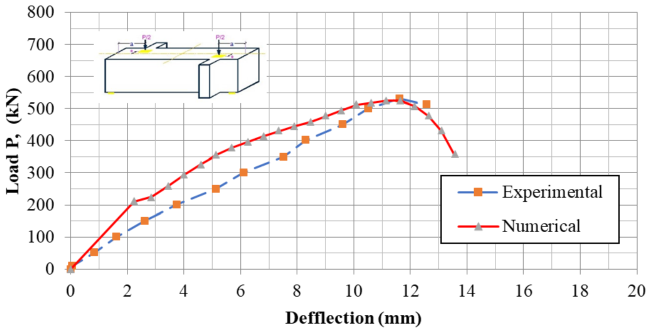

Figure 13 Load–deflection curve for the experimental and numerical results for specimen RB.5

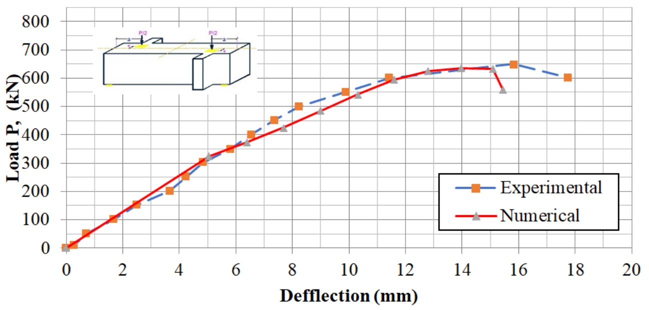

Figure 14 Load–deflection curve for the experimental and numerical results for specimen RB.6

4.4 The range of the studied parameters

For the parametric study, the concrete cylindrical compressive strength f_c` was explored across values of 20, 22.5, 25, 30, 35, and 40 MPa, while the area of GFRP (A_{GFRP} main) varied at 8Φ10, 8Φ12, 8Φ16, 8Φ20, 8Φ22, and 8Φ25. Also, the eccentricity of the load was studied using 150, 170, and 200 mm. External GFRP stirrups have diameters Φ8, Φ10, Φ12, and Φ16. Internal Vl. web RFT Φ8, Φ10, and Φ12. All specimens were subjected to a static vertical displacement applied at the center of the beam's bottom. The variables studied in the parametric investigation are detailed in Table 4.

Table 4 summarizes the results of the numerical parametric study conducted in this research. The ultimate loads and central deflections at ultimate load for various specimens were compared with those of the control specimen. The key findings are as follows:

- Effect of Concrete Compressive Strength ($f_{c'}$): The compressive strength of concrete significantly influences the shear strength capacity of beams reinforced with GFRP. Compared to the control model ($f_{c'}$ = 25, MPa), the failure load increased by: 13% for $f_{c'}$ = 30 MPa, 23% for $f_{c'}$ = 35, MPa, and 30% for $f_{c'}$ = 40 MPa.
- Effect of GFRP Reinforcement Area (A_f): Increasing the area of GFRP reinforcement (A_f) resulted in a proportional rise in the ultimate load. Compared to the control model with (A_f = 8F12), the ultimate load increased by:1% for (A_f = 16 mm), 10% for (A_f = 20, mm),12% for (A_f = 22, mm), and 18% for (A_f = 25, mm).
- Effect of Load Position (e): The influence of load position was evaluated using specimens RB.5 and **RB.6, which were tested with load positions at the top. Compared to the control specimen, the ultimate load exhibited a negligible reduction of: 6.2% for RB.5, and 3.8% for RB.6.

These findings emphasize the significant role of concrete compressive strength and GFRP reinforcement area in enhancing the load-carrying capacity, while changes in load position have minimal impact on ultimate load capacity.

Table 4 : Parametric study program: data and results

Studied parameters					
Model number	Studied variables		Numerical ultimate load P_u		Comments
	Value	Variable	Ultimate load, P_u (kN)	P_u/P_u control (-)	
RB.5	20	f_c` (MPa)	453.85	0.86	
	22.5		469.25	0.89	
	25		525.23	1.00	Control
	30		592.80	1.13	
	35		647.39	1.23	
	40		683.893	1.30	
RB.6	20	f_c` (MPa)	545.37	0.86	
	22.5		565.81	0.89	
	25		635.28	1.00	Control
	30		683.43	1.08	
	35		720.46	1.13	
	40		835.51	1.31	
RB.5	8Φ10	A_f(-)	508.53	0.97	
	8Φ12		525.23	1.00	Control
	8Φ16		531.53	1.01	
	8Φ20		581.43	1.10	
	8Φ22		591.29	1.12	
	8Φ25		621.59	1.18	

RB.6	8Φ10	A_f (-)	569.94	0.89	
	8Φ12		635.28	1.00	Control
	8Φ16		667.04	1.05	
	8Φ20		770.33	1.21	
	8Φ22		777.39	1.22	
	8Φ25		848.98	1.33	
RB.5	100	e (mm.)	850.44	1.62	
	150		525.23	1.00	Control
	200		505.23	0.96	
RB.6	100	e (mm.)	913.18	1.44	
	150		635.28	1.00	Control
	200		619.31	0.97	

4.4.1 Effect of compressive strength on the shear strength of GFRC beams

In this study, six different concrete compressive strengths were considered: 20, 22.5, 25, 30, 35, and 40 MPa. The effect of compressive strength on the load-carrying capacity and shear strength of GFRC beams was analyzed using ANSYS 15.0 software [33]. The results revealed a clear trend: as the grade of concrete strength increased, the predicted shear strength and load-carrying capacity of the beams also improved.

The load-deflection curves at the mid-span for box-section beams reinforced with longitudinal GFRP bars are presented in Figures 14 and 17, corresponding to the six compressive strengths. The results indicate that increasing the concrete strength enhanced the ultimate shear strength, load-carrying capacity, and ductility of the beams, as evidenced by Figures 15, 16, and the crack patterns illustrated in Figure 18 for specimen RB5.

Observations on Beam Behavior

All beam models exhibited two distinct phases of behavior:

Phase 1: Linear Elastic Behavior, in this phase, tensile stresses remained within the concrete's tensile strength limit. The beams showed linearly elastic behavior, characterized by high stiffness and low deflection.

Phase 2: Post-Cracking Behavior, this phase occurred when tensile stresses exceeded the tensile strength of the concrete, resulting in crack formation and a subsequent reduction in stiffness. The decrease in stiffness marked the transition from elastic to nonlinear behavior.

Increasing the concrete's compressive strength from 20 MPa to 40 MPa significantly enhanced the ability of the beams to withstand cracking loads and improved their overall performance. This improvement in shear strength and ductility highlights the role of higher concrete compressive strength in enhancing the structural integrity of GFRC beams.

These findings reinforce the importance of optimizing concrete compressive strength for achieving superior performance in reinforced concrete beams subjected to shear forces.

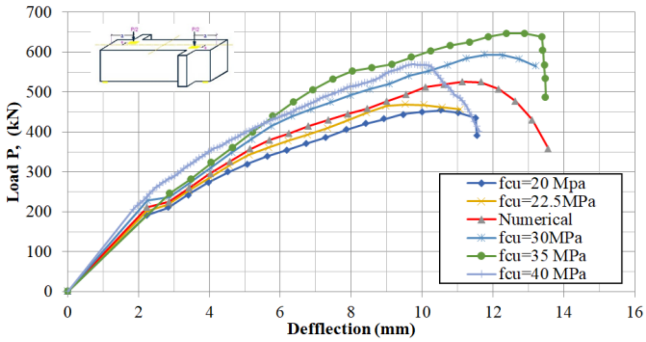

Figure 15 Numerical load–deflection curves for the effect of concrete compressive strength using specimen RB.5

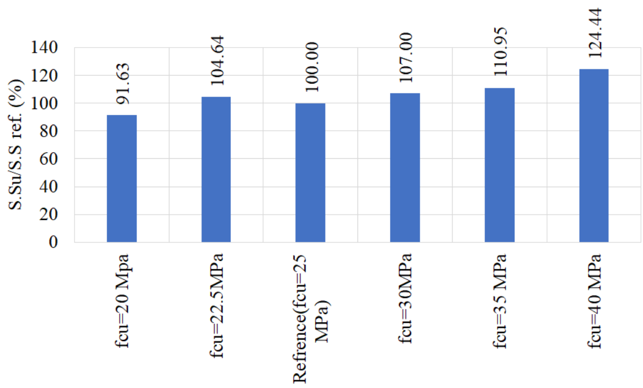

Figure 16 Numerical secant stiffness for the effect of concrete compressive strength using specimen RB.5 compared to the reference specimen

(a) (b)

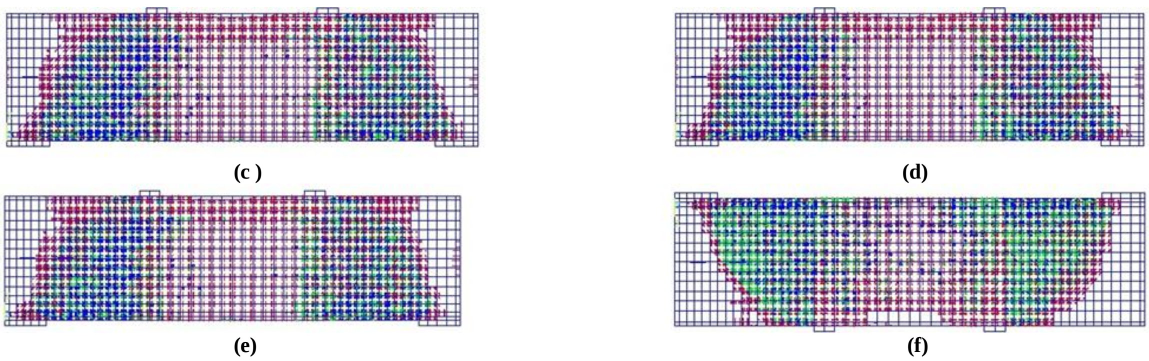

Figure 17 Cracking pattern of beams (a) fcu=20, (b) fcu=22.5, (b) fcu=22.5, (b) fcu=25, (b) fcu=30, (b) fcu=35 and (b) fcu=40

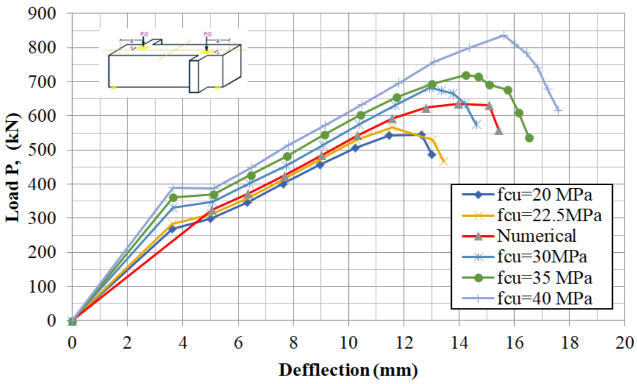

Figure 18 Numerical load–deflection curves for the effect of concrete compressive strength using specimen RB.6

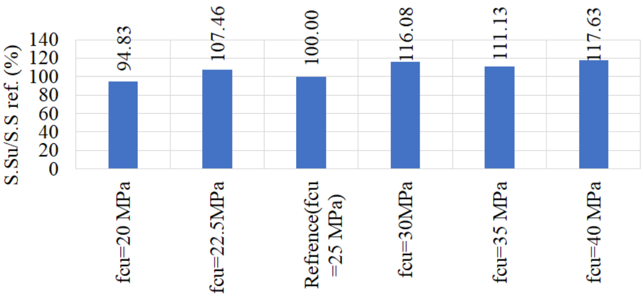

Figure 19 Numerical secant stiffness for the effect of concrete compressive strength using specimen RB.6 compared to the reference specimen.

4.4.2 Effect of strengthening reinforcement ratio (variation in the value of the bar diameter)

In this parametric study, three different diameters of shear-strengthening bent-up bars (8 mm, 10 mm, and 12 mm) were evaluated for their effect on the shear strength and load-carrying capacity of beams RB5 and RB6 using ANSYS software. The analysis demonstrated that increasing the diameter of the bent-up bars enhances the shear strength and stiffness of GFRC beams, with a corresponding increase in mid-span deflection at failure due to improved ductility.

The results, as shown in Figures 19 and 22, reveal an approximately linear increase in ultimate shear capacity and load-deflection response with increasing bar diameters. Additionally, Figures 20, 21, 23, and 25 highlight the influence of varying GFRP reinforcement ratios, achieved through changes in bar diameter, on the shear strength of the beams.

Key Observations:

- Beam RB5: Increasing the GFRP reinforcement diameter to 16 mm, 20 mm, 22 mm, and 25 mm** resulted in increases in ultimate shear strength by 1%, 10%, 12%, and 18%, respectively, compared to the baseline beam reinforced with 12 mm GFRP bars.
- Beam RB6: The same reinforcement diameters (16 mm, 20 mm, 22 mm, and 25 mm) increased the ultimate shear strength by 5%, 21%, 22%, and 11%, respectively, compared to the beam with 12 mm GFRP bars.

Finally, the study confirms that increasing the diameter of GFRP shear-strengthening bent-up bars significantly enhances the structural performance of GFRC beams. This improvement is reflected in higher shear capacity, increased stiffness, and improved ductility, highlighting the effectiveness of optimizing GFRP reinforcement ratios in reinforced concrete design.

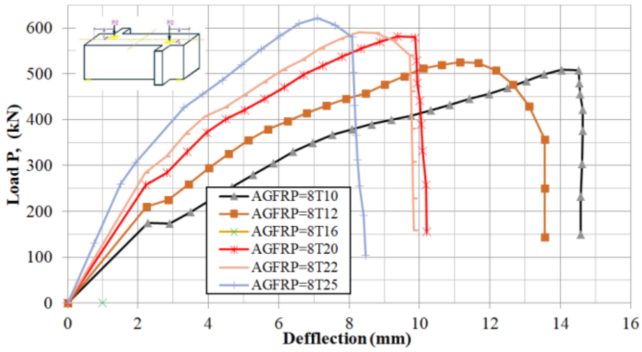

Figure 20 Numerical load-deflection curve for the effect of GFRP area for specimen RB5 (variation in the value of the bar diameter)

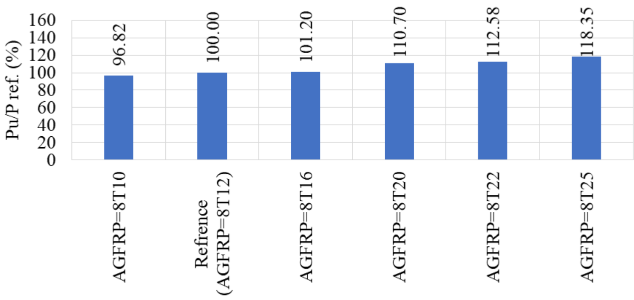

Figure 21 Numerical ultimate loads for the effect of GFRP area for specimen RB5 compared to the reference specimen (variation in the value of the bar diameter)

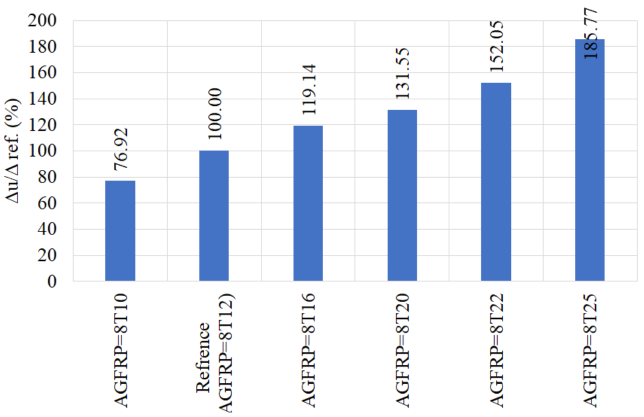

Figure 22 Numerical ultimate deflection for the effect of GFRP area for specimen RB5 compared to the reference specimen (variation in the value of the bar diameter)

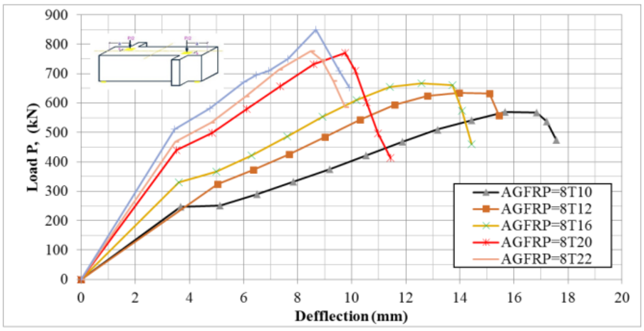

Figure 23 Numerical load-deflection curve for the effect of GFRP area for specimen RB6 compared to the reference specimen (variation in the value of the bar diameter)

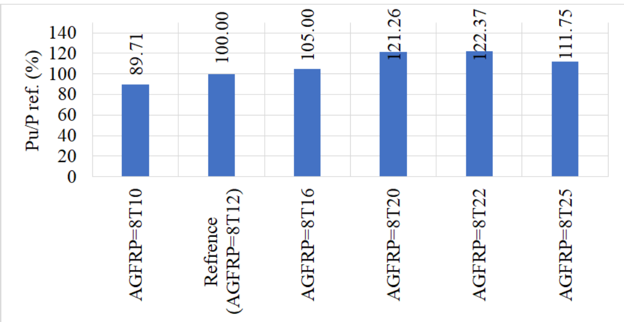

Figure 24 Numerical ultimate loads for the effect of GFRP area for specimen RB6 compared to the reference specimen (variation in the value of the bar diameter)

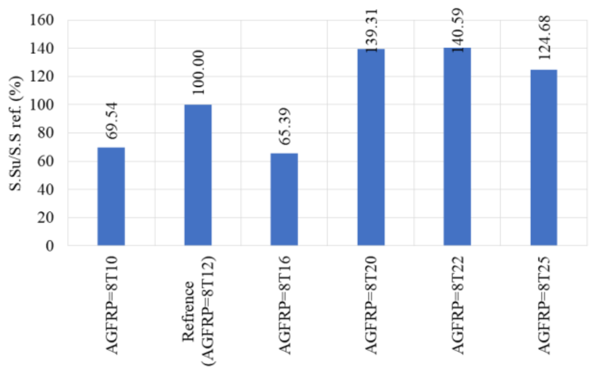

Figure 25 Numerical secant stiffness for the effect of external GFRP bars area for specimen RB5 compared to the reference specimen (variation in the value of the bar diameter)

4.4.3 The effect of the eccentricity of the loads (variation in the load eccentricity)

The effect of load eccentricity on a box-section reinforced concrete beam is a critical consideration in structural engineering, as it influences stress distribution, deflection, and overall structural behavior. Here's a detailed look at how load eccentricity affects such beams:

a. Stress distribution,
b. Axial load with eccentricity: when a load is applied eccentrically, it introduces direct compressive or tensile stress and bending stress due to the moment generated by the eccentricity,
c. Combined stress: The stress at any section of the beam will be the combination of axial stress (direct stress) and bending stress. This combined stress can be higher than the stress produced by a centrally applied load. figures 25 to 28 show the effect of the load eccentricity on the load-deflection curves, and the ultimate shear strength of the studied beams.

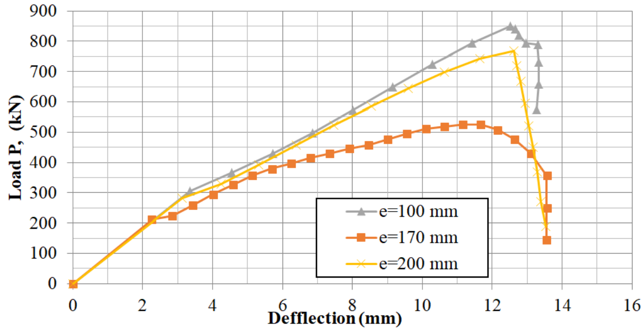

Figure 26 Load-deflection curves for the effect of eccentricity for specimen RB.5 (variation in the load eccentricity)

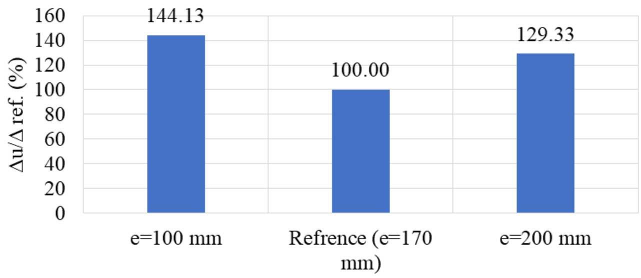

Figure 27 The effect of eccentricity on the numerical deflection at the ultimate load for specimen RB.5 compared to the reference specimen (variation in the load eccentricity)

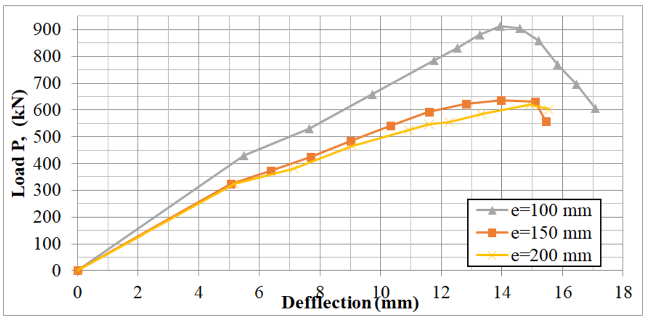

Figure 28 Load-deflection curves for the effect of eccentricity for specimen RB.6 compared to the reference specimen (variation in the load eccentricity)

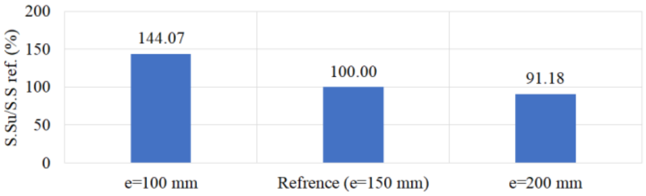

Figure 29 The effect of eccentricity on the numerical deflection at the ultimate load for specimen RB6 compared to the reference specimen (variation in the load eccentricity)

5. Conclusions

Nonlinear finite element analysis (NLFEA) was performed using ANSYS V15 [31] to simulate the behavior of simply supported reinforced concrete (RC) beams reinforced with glass fiber-reinforced polymer (GFRP) bars. The analysis focused on failure load, crack patterns, and load-deflection behavior. The findings provide valuable insights into the behavior of GFRP-reinforced RC simply suported beams, elucidating the impact of various parameters on their shear strength and overall performance. The following conclusions are drawn from the study:

1. The load-deflection curves and crack patterns predicted by the ANSYS program show good agreement with the experimental results, validating the reliability of the NLFEA model.
2. The ultimate load capacity predicted by ANSYS was slightly unconservative compared to experimental results, with an average ratio of (P_u^{ANSYS}/ $P_f^{Exp.}$ = 1.03). This deviation is attributed to the assumption of a perfect bond between concrete and GFRP bars in the numerical model.
3. The secant stiffness of the beams is highly sensitive to the diameter of the external GFRP stirrups, with improvements ranging from 36.10% to 219.6% within the studied parameters.
4. Optimized distribution of GFRP external stirrups significantly enhances beam ductility, increasing displacement ductility by 53.38% to 80.28%, while also raising the initial crack load.
5. Utilizing external GFRP stirrups significantly improves the toughness of the reinforced concrete specimens. The toughness enhancement for externally strengthened specimens ranges from 74.70% to 172.93%, underscoring the efficacy of this strategy.
6. The orientation of the NSM GFRP external stirrups greatly impacts the ultimate load capacity. Inclined stirrups (45°) outperform vertical stirrups, with a 27% improvement in load-carrying capacity. The use of inclined stirrups transforms the failure mode from brittle shear to ductile failure, demonstrating their superiority.
7. The shear strength of the beams is strongly affected by changes in the GFRP bar diameter, Increasing the bar diameter from 10 mm to 12 mm enhances the load-carrying capacity by 5%. Reducing the bar diameter from 10 mm to 8 mm results in a 10% decrease in load-carrying capacity.
8. This study demonstrates the effectiveness of external GFRP reinforcement, particularly through optimized stirrup orientation and diameter, in enhancing the structural performance of RC beams. The findings highlight the potential of GFRP as a reliable material for shear strengthening, improving ductility, stiffness, toughness, and load-carrying capacity.

REFERENCES

[1] Noel, M., Soudki, K., 2011. Evaluation of FRP post-tensioned slab bridge strips using AASHTO-LRFD bridge design specifications. J. Bridge Eng. 16, 839e846.

[2] Elkareim, S.S.A., Moustafa, O., 2011. Experimental analysis of R.C. beam strengthened with discrete glass fiber. Arch. Civil Eng. 9, 205e215, 2011.

[3] Soliman, A.E.S., Osman, M., 2011. Efficiency of Using Discrete Fibers on the Shear Behavior of R.C. Beams. Production and Hosting by Elsevier B.V. All Rights Reserved.

[4] Abdul-Zaher, A.S., Abdul-Hafez, L.M., Tawfic, Y.R., Hammed, O., 2016. Shear behavior of fiber reinforced concrete beams. J. Eng. Sci. 44, 132e144.

[5] Ahmadi, M., Kheyroddin, A., Dalvan, A., Kioumarsi, M., 2020. New empirical approach for determining the nominal shear capacity of steel fiber reinforced concrete beams. Construct. Build. Mater. 234, 117293.

[6] Siddika, A., Abdullah AlMamun, M., Alyousef, R., Mugahed Amran, Y.H., 2019. Strengthening of reinforced concrete beams by usingfiber-reinforced polymercomposites. J. Build. Eng. 25, 100798.

[7] Jin, L., Xia, H., Jiang, X.A., Du, X., 2020. Size effect on shear failure of CFRP-strengthened concrete beams without web reinforcement. Compos. Struct. 236, 111895.

[8] Pang, L., Qu, W., Zhu, P., Xu, J., 2016. Design propositions for hybrid FRP-steel reinforced concrete beams. J. Compos. Construct. 20, 04015086.

[9] Monika, K., Renata, K., Joaquim, A.O., 2017. Influence of longitudinal GFRP reinforcement ratio on the shear capacity of concrete beams without stirrups. Procedia Eng. 193, 361e368.

[10] Seo, S.-Y., Lee, M.S., Feo, L., 2016. Flexural analysis of RC beam strengthened by partially de-bonded NSM FRP strip. Compos. B Eng. 101, 21e30.

[11] Panahi, M., Izadinia, M., 2018. A parametric study on the flexural strengthening of reinforced concrete beams with near surface mounted FRP bars. Civ. Eng. J 4, 8.

[12] Khalifa, A.M., 2016. Flexural performance of RC beams strengthened with near-surface mounted CFRP strips. Alex. Eng. J. 55, 1497e1505.

[13] Zhanga, S.S., Yua, T., Chen, G.M., 2017. Reinforced concrete beams strengthened in flexure with near-surface mounted (NSM) CFRP strips. Compos. B Eng. 131, 30e42.

[14] De Lorenzis, L., Teng, J., 2007. Near-surface mounted FRP reinforcement: an emerging technique for strengthening structures. Compos. B Eng. 38, 119e143.

[15] El-Hacha, R., Rizkalla, S.H., 2004. Near-surface-mounted fiber reinforced polymer reinforcements for flexural strengthening of concrete structures. ACI Struct. J. 101, 717e726.

[16] Amin Saleh, Ahmed Fathy, Ahmed Farouk, Moaz Nasser, "Performance of Steel Fiber Reinforced Concrete Corbels", Published in International Research Journal of Innovations in Engineering and Technology (IRJIET), Volume 3, Issue 2, pp 22-27, February 2019. https://irjiet.com/Volume-3/Issue-2-February-2019/Performance-of-Steel-Fiber-Reinforced-Concrete-Corbels/39

[17] Ahmad H., Elnemr A., Ali N., Hussain Q., Chaiyasarn K., and Joyklad P. (2021), Finite element analysis of glass fiber-reinforced polymer-(GFRP) reinforced continuous concrete beams, Polymers 13, 4468 http://dx.doi.org/10.3390/polym13244468

[18] Tahenni T., Bouziadi F., Boulekbache B., and Amziane S. (2021), Experimental and numerical investigation of the effect of steel fibers on the deflection behavior of reinforced concrete beams without stirrups. Structures, 33, 1603-1619 http://dx.doi.org/10.1016/j.istruc.2021.05.005

[19] Barour S., Zergua A., Bouziadi F., Kaloop M.R., and El Demerdash W.E. (2022), Nonlinear numerical and analytical assessment of the

shear strength of RC and SFRC beams externally strengthened with CFRP sheets, Advanced Civil Engineering, 8741158 http://dx.doi.org/10.1155/2022/8741158

[20] Hany M., Makhlouf M.H., Ismail G., and Debaiky A.S. (2022), Experimental shear strengthening of GFRC beams without stirrups using innovative techniques, Structures Engineering Mechanics, 83, 415-433 http://dx.doi.org/10.12989/sem.2022.83.4.415

[21] Ebrahim E.A., Mahmoud A.A., Salama M.A., and Khater A.N. (2024), Shear behavior of box-section concrete beams reinforced by FRP bars and FRP stirrups, Structural Concrete, https://doi.org/10.1002/suco.202300129.

[22] Elavenil, S., & Chandrasekar, V. (2022). Analytical and finite element analysis of RC beams retrofitted with FRP composites under torsion. International Journal of Applied Engineering Research, 13(1), 1-12. https://doi.org/10.1111/j.1747-1567.2022.15862.x

[23] Vasudevan, G., & Kothandaraman, S. (2023). Parametric study on the torsional behavior of reinforced concrete beams strengthened with FRP bars using finite element analysis. Strength of Materials, 45(2), 231-241. https://doi.org/10.1007/s11223-023-1568-2

[24] Dazulhisham, M. A. S., Abdul Halim, M. A. I., & Goh, L. D. (2024). Near-surface Mounted Technology in Strengthening Reinforced Concrete Beam. International Journal of Sustainable Construction Engineering and Technology, 15(1), 211-225. https://publisher.uthm.edu.my/ojs/index.php/IJSCET/article/view/17051

[25] Tahenni, T., Bouziadi, F., Boulekbache, B., Amziane, S., 2021. Experimental and numerical investigation of the effect of steel fibers on the deflection behavior of reinforced concrete beams without stirrups. Structures 33, 1603e1619.

[26] Bouziadi, F., Boulekbache, B., Haddi, A., Djelal, C., 2018a. Experimental and finite element analysis of creep behavior of steel fiber reinforced high strength concrete beams. Construct. Build. Mater. 173, 101e110.

[27] Bouziadi, F., Boulekbache, B., Haddi, A., Djelal, C., Hamrat, M., 2018b. Numerical analysis of shrinkage of steel fiber reinforced high-strength concrete subjected to thermal loading. Construct. Build. Mater. 181, 381e393.

[28] Hamrat, M., Bouziadi, F., Boulekbache, B., Daouadji, T.H., Chergui, S., Labed, A., et al., 2020. Experimental and numerical investigation on the deflection behavior of pre-cracked and repaired reinforced concrete beams with fiber-reinforced polymer. Construct. Build. Mater. 249, 118745.

[29] Lahmar, N., Bouziadi, F., Boulekbache, B., Meziane, E.-H., Hamrat, M., Haddi, A., 2020. Experimental and finite element analysis of shrinkage of concrete made with recycled coarse aggregates subjected to thermal loading. Construct. Build. Mater. 247, 118564.

[30] Mahmoud A.M. (2015), Finite element implementation of punching shear behaviors in shear-reinforced flat slabs. Ain Shams Engineering Journal, 6(3), 735-754. https://doi.org/10.1016/j.asej.2014.12.015

[31] Mahmoud, A., Nasser, M., Mostafa, T., & Khater, A. (2023). Retrofitting of Box Section Concrete Beams to Resist Shear and Torsion Using Near-Surface-Mount (NSM) GFRP Stirrups. Fracture and Structural Integrity, 18(67), 319–336. https://doi.org/10.3221/IGF-ESIS.67.23

[32] Martinez S., Nilson A. H., and Slate F. (1984), Spiral-reinforced high-strength concrete columns. ACI Structural Journal, (81) 5, 431-442. http://dx.doi.org/10.14359/10693

[33] Manual, F.L.U.E.N.T. (2015). ANSYS Release Version 15.0. User's Guide. ANSYS 15 Manual Set, ANSYS Inc., South Pointe Technology Drive, FLEXLM License, Manager, Canonsburg, PA, U.S.A., 2015. https://forum.ansys.com/uploads/846/SCJEU0NN8IHX.pdf.

[34] Egyptian Code of Practice for Design and Construction of Reinforced Concrete Structures, ECP-208 (2019), Housing and Building Research Center, Ministry of Building and Construction, Giza, Egypt (2019), Chapter 4, 25-32. https://www.cuipcairo.org/en/directory/housing-building-national-research-center

[35] Egyptian Code of Practice for Design and Construction of Reinforced Concrete Structures, ECP-203. (2019). Housing, and Building Research Center, Ministry of Building and Construction, Giza, Egypt, Chapter 6,113-122. https://www.cuipcairo.org/en/directory/housing-building-national-research-center

[36] ASTM D7205 (2019): Tensile Tests of GFRP Matrix Composite Bars. https://www.parsros.net/urun/astm-d7205-standard-test-method-for-tensile-properties-of-fiber-reinforced-polymer-matrix-composite-bars-2/#:~:text=ASTM%20D7205%20%E2%80%93%20This%20test%20method%20determines%20the,tensile%20elements%20in%20reinforced%2C%20prestressed%2C%20or%20post-tensioned%20concrete

[37] ASTM D790-02 (1998), Standard Test Methods for Flexural Properties of Unreinforced and Reinforced Plastics and Electrical Insulating Materials, American Society of Mechanical Engineering, New York, http://dx.doi.org/10.1520/D0790-02